Neural inverse optimal control applied to design therapeutic options for patients with COVID-19

Victor M. Chan
Electrical Engineering Department
CINVESTAV-IPN
Guadalajara, México
Victor.Chan@cinvestav.mx

Esteban A. Hernández-Vargas
Institute of Mathematics
UNAM
Querétaro, México
esteban@im.unam.mx

Edgar N. Sánchez
Electrical Engineering Department
CINVESTAV-IPN
Guadalajara, México
sanchez@gdl.cinvestav.mx

2021 International Joint Conference on Neural Networks (IJCNN) | 978-1-6654-3900-8/21/$31.00 ©2021 IEEE | DOI: 10.1109/IJCNN52387.2021.9534240

***Abstract*—In this paper we apply an inverse optimal controller (IOC) based on a control Lyapunov function (CLF) to schedule theoretical therapies for the novel coronavirus disease (COVID-19). This controller can represent the viral dynamics of Severe Acute Respiratory Syndrome Coronavirus 2 (SARS-CoV-2) in the host. The virus dynamics consider the antiviral effects and immune responses as control inputs. The proposed controller is based on a Recurrent High Order Neural Network (RHONN) used as an identifier trained with Extended Kalman Filter (EKF). Simulations show that applying treatment 2 days post symptoms would not significantly alter the viral load. The proposed controller to stimulate the immune response displays a better effectiveness compared to the effectiveness displayed by the antiviral effects.**

***Index Terms*—Recurrent High-Order Neural Networks, Neural Networks, COVID-19, Inverse Optimal Control, Extended Kalman Filter**

I. Introduction

The Severe Acute Respiratory Syndrome Coronavirus 2 (SARS-CoV-2) is the virus causing the novel coronavirus disease (COVID-19) that has paralyzed the world, affecting the economy of many countries and causing many losses of human lives; having until today February 1st, 2021, more than 100 million people infected and more than 2 million confirmed deaths [1]. Researchers have tried to contribute from different areas of knowledge, new ways to study the virus, the disease and provide solutions.

These contributions have been from a practical and theoretical point of view, with promising results. Several models that have been proposed about the spread of the virus around the globe [2] [3] and [4]. Although it is important to know the behavior of the virus spread, it is also relevant to know the virus dynamics in the host, in order to develop possible medical strategies once antivirals are available against COVID-19. For this reason we will synthesized a control law that will allow us to develop these medical strategies.

In the model presented in [5], the effects of antivirals and the stimulation of the immune response are included as possible therapies to decrease the viral load, so these will be used as our control inputs to synthesize the control law. Currently, control techniques have been applied to mitigate the spread of SARS-CoV-2 as in [4], [7] and [8]. Another control techniques have also been used to develop therapeutic options for other viruses such as Influenza [9] and HIV [10].

In this paper we propose the application of an optimal control law for a nonlinear system. To obtain the algorithm for this system, the solution of a Hamilton-Jacobi-Bellman (HJB) partial differential equation is required. Even if the solution of the HJB equation exists, it may be very difficult to find or may not exist [11]. To solve this problem without the need to solve the HJB equation, the inverse optimal control (IOC) technique uses a control Lyapunov function (CLF), which guarantees system stability. The CLF is used to define a cost functional, witch then is minimized as shown in [12].

For a controller based on a plant model, the desired performance may not be obtained due to disturbances, uncertain parameters or unmodeled dynamics. For this reason, the use of a discrete time recurrent high order neural network (RHONN) as an identifier allows us to approximate a mathematical model of the plant even in the presence of uncertainties and modeling errors. A RHONN model is easy to implement and has a relatively simple structure [13] and [14].

To train this neural network, the Extended Kalman Filter (EKF) algorithm is used. EKF provides a recursive optimal estimator for the neural weights as shown in [15], [16], [17], [18], [19] and [20] . The EKF will allow us to perform online training and minimize the identification error by finding the optimal value of the RHONN weights. With this, a controller based on a RHONN model will allow us to increase its robustness. In recent years recurrent neural networks trained with the EKF have shown to have many practical and reliable applications [9], [11], [21] and [22].

The structure of this paper is organized as follows. In section II the RHONN identifier and EKF algorithm are introduced. Then in section III the inverse optimal control is described. In section IV the mathematical model is presented, the neural model identification is proposed and neural inverse optimal control laws for viral dynamics are developed. Simulations results are presented in section V. Finally the conclusions are stated in section VI.

II. Fundamentals

A. Recurrent High Order Neural Networks

Let us consider the following discrete time nonlinear system:

$$x_{k+1} = f(x_k) + g(x_k)u_k \tag{1}$$

where $x \in \Re^n$ which is the state of the system at time $k \in \mathcal{N}$. $u \in \Re^m$ is the control input, $f : \Re^n \to \Re^n$ and $g : \Re^n \to \Re^m$ are smooth mappings. The identifier model is described as:

$$\hat{x}_{i,k+1} = w_i^T \phi(\hat{x}_k, u_k), \qquad i = 1, \dots n \tag{2}$$

where $\hat{x}_i \in \Re^L$ is the state of the i-th neuron which identifies the i-th component of state vector, $u \in \Re^{L_i}$ is the input vector of the neural network, and ϕ_i is defined as:

$$\phi_i(x_k, u_k) = \begin{bmatrix} \phi_{i_1} \\ \phi_{i_2} \\ \vdots \\ \phi_{i_{L_i}} \end{bmatrix} = \begin{bmatrix} \prod_{j \in I_1} \xi_{ij}^{dij(1)} \\ \prod_{j \in I_2} \xi_{ij}^{dij(2)} \\ \vdots \\ \prod_{j \in I_{L_i}} \xi_{ij}^{dij(L_i)} \end{bmatrix} \tag{3}$$

where $d_{ij,k}$ are nonnegative integers. L_i is the respective number of high orders connections. $I_1, I_2, \dots, I_{L_i}$ is a collection of nonordered subsets of $1, 2, \dots, n+m$ where n is the state dimension, m is the number of external inputs, and ξ_i is defined as:

$$\xi_i = \begin{bmatrix} \xi_{i_1} \\ \xi_{i_2} \\ \vdots \\ \xi_{i_n} \\ \xi_{i_{n+1}} \\ \vdots \\ \xi_{i_{n+m}} \end{bmatrix} = \begin{bmatrix} S(x_1) \\ \vdots \\ S(x_n) \\ u_1 \\ \vdots \\ u_m \end{bmatrix} \tag{4}$$

where $S(\cdot)$ is an activation function defined as

$$S(\varsigma) = \mu_i \tanh(\beta_i \varsigma) \tag{5}$$

with ς represents any real variable value, μ, and β are positive constants.

The hyperbolic tangent function is used in this work since the antisimetric functions allow the neural network to learn the process dynamic faster than other activation functions.

B. Extended Kalman Filter Training algorithm

For RHONN training an EKF is used, which leads to determine the optimal RHONN weights values for minimizing the prediction error. The EKF based algorithm is given as

$$\begin{aligned} K_{i,k} &= P_{i,k} H_{i,k} M_{i,k} \\ w_{i,k+1} &= w_{i,k} + \eta_i K_{i,k} e_{i,k} \\ P_{i,k+1} &= P_{i,k} - K_{i.k} H_{i,k}^T P_{i,k} + Q_{i,k} \end{aligned} \tag{6}$$

with:

$$M_{i,k} = [R_{i,k} + H_{i,k}^T P_{i,k} H_{i,k}]^{-1} \tag{7}$$

$$e_{i,k} = x_{i,k} - \hat{x}_{i,k} \tag{8}$$

$$H_{i,k} = \left[\frac{\partial \hat{x}_{i,k}}{\partial w_{ij,k}} \right]^T \tag{9}$$

where $i = 1, \dots, n$ and $j = 1, \dots, L_i$. $\hat{x}_{i,k}$ is the ith neural network state. $x_{i,k}$ is the ith plant state. $e_{i,k} \in \Re$ is the respective identification error. $K_i \in \Re^{L_i \times m}$ is the Kalman gain matrix. $P_{i,k} \in \Re^{L_i \times L_i}$ is the prediction error associated covariance matrix at the step k. $w_i \in \Re^{L_i}$ is the weight vector considered as state of the network. $Q_i \in \Re^{L_i \times L_i}$ is the state noise associated covariance matrix. $H_i \in \Re^{L_i \times m}$ is a matrix where each entry H_{ij} is the derivate of one of the neural network states $\hat{x}_i$, respect to one neural network weight w_{ij}. $R_i \in \Re^{m \times m}$ is the measurement noise associated covariance matrix. η_i is a design parameter.

Commonly P_i and Q_i are initialized as diagonal matrices. The convergence analysis, for RHONN identifier trained with EKF learning is studied in [22].

III. Inverse Optimal Control

In this section optimal control methodology and its properties are briefly discusses. Let consider the following discrete-time nonlinear system:

$$x_{k+1} = f(x_k) + g(x_k)u_k, \qquad x_0 = x(0) \tag{10}$$

where $x \in \Re^n$ which is the state of the system at time $k \in \mathcal{N}$. $u \in \Re^m$ is the control input, $f : \Re^n \to \Re^n$ and $g : \Re^n \to \Re^m$ are smooth mappings. The tracking error is defined as follows

$$z_k = x_k - x_{\delta,k} \tag{11}$$

with $x_{\delta,k}$ as the desired trajectory and $z_k \in \Re^n$. The error dynamics one step ahead is calculated as

$$\begin{aligned} z_{k+1} &= x_{k+1} - x_{\delta,k+1}, \qquad z(0) = z_0 \\ z_{k+1} &= f(x_k) + g(x_k)u_k - x_{\delta,k+1} \end{aligned} \tag{12}$$

For minimization of the error associated with trajectory tracking of system (12), an optimal control law u_k is already proposed respecting the following cost functional

$$J(z_k) = \sum_{n=k}^{\infty} \left(l(z_n) + u_n^T R(z_n) u_n \right), \qquad J(0) = 0 \tag{13}$$

with $J(z_k) : \Re^n \to \Re$, $l(z_k) : \Re^n \to \Re^+$ is a positive semidefinite function, and $R(z_k) : \Re^n \to \Re^{m \times m}$, $R(z_k) = R^T(z_k) > 0$ is a matrix-valued function for all x_k defined in [23]. Then:

$$\begin{aligned} J(z_k) &= l(z_k) + u_k^T R(z_k) u_k + \sum_{n=k+1}^{\infty} \left(l(z_n) + u_n^T R(z_n) u_n \right) \\ J(z_k) &= l(z_k) + u_k^T R(z_k) u_k + J(z_{k+1}) \\ J^\star(z_k) &= \min_{u_k} \left(l(z_k) + u_k^T R(z_k) u_k + J^\star(z_{k+1}) \right) \end{aligned} \tag{14}$$

Assuming that the full state x_k is available. Then, using the optimal function $J^\star(x_k)$ in (14) as a Lyapunov function $V(x_k)$, so (14) can be rewritten as

$$V(z_k) = \min_{u_k} \left(l(z_k) + u_k^T R(z_k) u_k + V(z_{k+1}) \right) \tag{15}$$

If the boundary condition $V(0) = 0$ is fulfilled hence, $V(z_k)$ must be a Lyapunov function and its value one step ahead depends on both z_k and u_k by means of z_{k+1}. For the finite horizon optimization case, in Bellman optimality principle [24], [25], the function $V(z_k)$ satisfies the discrete-time Bellman equation [25], [26] and [27].

In order to establish the conditions of the optimal control law, a discrete-time Hamiltonian function is used as follows

$$\mathcal{H}(z_k, u_k) = l(z_k) + u_k^T R(z_k) u_k + V(z_{k+1}) - V(z_k) \tag{16}$$

The optimal control law should satisfy the following condition

$$\frac{\partial \mathcal{H}(z_k, u_k)}{\partial u_k} = 0 \tag{17}$$

then,

$$\begin{aligned} 0 &= 2R(z_k)u_k + \frac{\partial V(z_{k+1})}{\partial u_k} \\ 0 &= 2R(z_k)u_k + \frac{\partial z_{k+1}}{\partial u_k}\frac{\partial V(z_{k+1})}{\partial z_{k+1}} \\ 0 &= 2R(z_k)u_k + g^T(x_k)\frac{\partial V(z_{k+1})}{\partial z_{k+1}} \end{aligned}$$

Hence, trajectory tracking using optimal control law is defined as

$$u_k^\star = -\frac{1}{2} R^{-1}(z_k) g^T(x_k) \frac{\partial V(z_{k+1})}{\partial z_{k+1}}, \quad V(0) = 0 \tag{18}$$

In order to solve the HJB equation in (18) for reaching the trajectory, an inverse optimal control approach is defined as follows

Definition 1. Consider the tracking error as (11). The control law is defined in (18) will be inverse optimal stabilizing along the desired trajectory $x_{\delta,k}$ if :

1) for system (10) achieves (global) asymptotic stability of $x_k = 0$, along reference $x_{\delta,k}$ and;
2) $V(z_k)$ is (radially unbounded) positive definite function such that the inequality

$$\bar{V} := V(z_{k+1}) - V(z_k) + u^{\star T}_k R(z_k) u^\star{}_k \leq 0,$$

is satisfied.

Selecting $l(z_k) := -\bar{V}$, the cost functional (13) is minimized, where, V is a solution for Hamiltonian function (16).

In order to satisfy the conditions (1) and (2) in *Definition* 1, a quadratic candidate control Lyapunov function (CLF) $V(z_k)$ takes the following form

$$V(z_k) = \frac{1}{2} z_k^T P z_k \tag{19}$$

with $P = P^T > 0$, in order to ensure stability of the tracking error (11). Substituting (19) in the optimal control law (18), we obtain

$$u_k^\star = -\frac{1}{2} R^{-1}(z_k) g^T(x_k) \frac{\partial (z_{k+1}^T P z_{k+1})}{\partial z_{k+1}} \tag{20}$$

Knowing that biological systems are usually positives, i. e. states, inputs and outputs are always nonnegative. The optimal control law for nonnegative systems is described as follows

$$u_k^\star = \left| -\frac{1}{2} (R(z_k) + P_2(x_k))^{-1} P_1(x_k, x_{\delta,k}) \right| \tag{21}$$

with

$$P_1(x_k, x_{\delta,k}) = \begin{cases} g^T(x_k) P (f(x_k) - x_{\delta,k+1}) \\ \quad \text{for} \quad f(x_k) \geq x_{\delta,k+1} \\ \\ g^T(x_k) P (x_{\delta,k+1} - f(x_k)) \\ \quad \text{for} \quad f(x_k) \leq x_{\delta,k+1} \end{cases} \tag{22}$$

$$P_2(x_k) = \frac{1}{2} g^T(x_k) P g(x_k) \tag{23}$$

and

$$R(z_k) = \frac{x_k^T r x_k}{\left\| x_{\delta,k+1} \right\|} \tag{24}$$

where $P_1(x_k, x_{\delta,k})$, $P_2(x_k)$ and r positive definite symmetric matrices, therefore $(R(z_k) + P_2(x_k)) > 0$. With these conditions the inverse matrix in (21) is ensured.

IV. Mathematical Model

According to [5] we consider a virus model that describes the SARS-CoV-2 dynamics and T cell response against SARS-CoV-2. In this model it is assumed that T cell proliferation (T) is induced by viral load (V) as follows

$$\frac{dV}{dt} = pV\left(1 - \frac{V}{K}\right) - c_T V T - cV \tag{25}$$

$$\frac{dT}{dt} = s_T + rT\left(\frac{V^n}{V^n + k_T^n}\right) - \delta_T T \tag{26}$$

where, V is the SARS-CoV-2 viral load ($\log_{10}$ copies/mL), T is the number of effector T cells, p is the replication rate per day, K is the maximum carrying capacity, c_T is the rate of virus elimination, c is the viral clearance, s_T is the T cell homeostasis, r is the maximum activation rate, δ_T is the half life of T cells. The activation of T cell proliferation by the virus follows a log-sigmoidal form with k_T as half saturation constant and the coefficient n relates to the width of the sigmoidal function.

This model was fitted as shown in [5] with patient data presented in [6]. It is important to highlight that in this model the maximum peak of T cells is achieved between 5 to 10 day post-symptoms onset. Due to the similarities between the influenza virus and SARS-CoV-2, in this paper it will consider the medical therapies that in [9] are used to decrease the viral load. Antivirals, that inhibit one or more parts of the viral cycle are shown in Fig. 1. Immune therapies can help the host

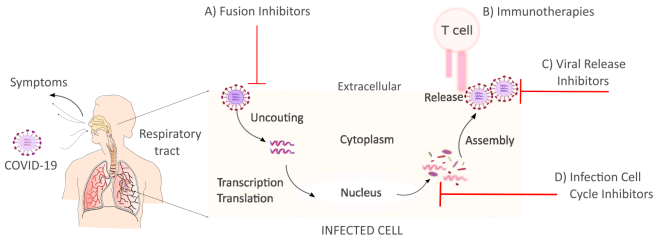

Fig. 1. **Replication Cycle of SARS-CoV-2.** The virus RNA is uncoated in the cytoplasm after the binding to receptors of the host cell. Then, to generate new viral RNA material and proteins, the transcription/translation processes take place. The virus is released after the assembly occurs within vesicles. After that, the virus can infect other cells, once is released. This cycle is presented in [5].

to fight a disease or infection. This therapies promote T-cell proliferation.

The therapies described above are included in the model proposed in (25-26), so that the following model is proposed

$$\frac{dV}{dt} = (1-u_r)pV\left(1-\frac{V}{K}\right) - c_T VT - cV \tag{27}$$

$$\frac{dT}{dt} = s_T + u_m rT\left(\frac{V^n}{V^n+k_T^n}\right) - \delta_T T \tag{28}$$

where, u_r is the antiviral effects and u_m is the immune modulation.

To establish a control law, the terms in (27-28) are simplifying as follows

$$\dot{x}_1 = a_1x_1 - a_2x_1^2 - a_3x_1x_2 - \left(a_4x_1 - a_2x_1^2\right)u_r \tag{29}$$

$$\dot{x}_2 = b_1 - b_2x_2 + b_3\left(\frac{x_1^2x_2}{x_1^2+b_4^2}\right)u_m \tag{30}$$

where, $x_1 = V$, $x_2 = T$, $a_1 = p - c$, $a_2 = \dfrac{p}{K}$, $a_3 = c_T$, $a_4 = p$, $b_1 = s_T$, $b_2 = \delta_T$, $b_3 = r$ and $b_4 = k_T$.

From continues-time system described in (29-30) a discrete-time system is calculated using Euler method as follows:

$$x_{1,k+1} = x_{1,k} + T_s\Big[a_1x_{1,k} - a_2x_{1,k}^2 - a_3x_{1,k}x_{2,k} - (a_4x_{1,k} - a_2x_{1,k}^2)u_{r,k}\Big] \tag{31}$$

$$x_{2,k+1} = x_{2,k} + T_s\left[b_1 - b_2x_{2,k} + b_3\left(\frac{x_{1,k}^2x_{2,k}}{x_{1,k}^2+b_4^2}\right)u_{m,k}\right] \tag{32}$$

The following parallel RHONN is proposed considering discrete-time viral dynamics as in (31-32)

$$\hat{x}_{1,k+1} = w_{11}S(\hat{x}_{2,k}) + w_{12}S(\hat{x}_{1,k})S(\hat{x}_{2,k}) + \left[w_{13}S(\hat{x}_{1,k}) + w_{14}S(\hat{x}_{2,k})\right]u_{r,k} \tag{33}$$

$$\hat{x}_{2,k+1} = w_{21}S(\hat{x}_{2,k}) + w_{22}S(\hat{x}_{1,k})u_{m,k} \tag{34}$$

Now we analyze each control input separately to compare their performance in the viral system (27-28).

A. Neural Inverse Optimal Control

To determine a control law that allows us to analyze antiviral effects (u_r), we set $u_m = 1$ in the proposed neural identifier in (33) and (34) as follows:

$$\hat{x}_{1,k+1} = w_{11}S(\hat{x}_{2,k}) + w_{12}S(\hat{x}_{1,k})S(\hat{x}_{2,k}) + \left[w_{13}S(\hat{x}_{1,k}) + w_{14}S(\hat{x}_{2,k})\right]u_{r,k} \tag{35}$$

$$\hat{x}_{2,k+1} = w_{21}S(\hat{x}_{2,k}) + w_{22}S(\hat{x}_{1,k}) \tag{36}$$

These equations can be described as a nonlinear system as in (10) as follows

$$f_r(\hat{x}_k) = \begin{bmatrix} w_{11}S(\hat{x}_{2,k}) + w_{12}S(\hat{x}_{1,k})S(\hat{x}_{2,k}) \\ w_{21}S(\hat{x}_{2,k}) + w_{22}S(\hat{x}_{1,k}) \end{bmatrix} \tag{37}$$

and,

$$g_r(\hat{x}_k) = \begin{bmatrix} w_{13}S(\hat{x}_{1,k}) + w_{14}S(\hat{x}_{2,k}) \\ 0 \end{bmatrix} \tag{38}$$

On the other hand a RHONN model for immune response (u_m) is described as follows by setting $u_r = 0$

$$\hat{x}_{1,k+1} = w_{11}S(\hat{x}_{2,k}) + w_{12}S(\hat{x}_{1,k})S(\hat{x}_{2,k}) \tag{39}$$

$$\hat{x}_{2,k+1} = w_{21}S(\hat{x}_{2,k}) + w_{22}S(\hat{x}_{1,k})u_{m,k} \tag{40}$$

Additionally, immune response RHONN model (39-40) can be rewritten as follows

$$f_m(\hat{x}_k) = \begin{bmatrix} w_{11}S(\hat{x}_{2,k}) + w_{12}S(\hat{x}_{1,k})S(\hat{x}_{2,k}) \\ w_{21}S(\hat{x}_{2,k}) \end{bmatrix} \tag{41}$$

and,

$$g_m(\hat{x}_k) = \begin{bmatrix} 0 \\ w_{22}S(\hat{x}_{1,k}) \end{bmatrix} \tag{42}$$

Now a control law for each input can be synthesized as in (21). In both cases for control law we set the desired trajectory $x_\delta = 0$. For u_r the following parameters are set as follows $P = \begin{bmatrix} 2.16 & 0 \\ 0 & 0.0036 \end{bmatrix}$ and $R = 1$. For u_m $P = \begin{bmatrix} 0.0001 & 0 \\ 0 & 0.000015 \end{bmatrix}$ and $R = 1$ were selected.

V. Simulation Results

This section presents results obtained via simulations. The EKF initial values for antivirals are selected as diagonal matrices with the following nonzero elements: $P_{1,0} = 1\times10^6$, $P_{2,0} = 1\times10^3$, $Q_1 = 100$, $Q_2 = 1000$, $R_1 = 1$, $R_2 = 10000$, $\eta_1 = 0.91$ and $\eta_2 = 0.34$.

TABLE I
VIRAL DYNAMIC PARAMETERS

Parameter	*Nominal Value*	*Units*
p	6.31	1/day
K	7.7451×10^7	log10 copies/mL
c_T	1.58×10^{-6}	(1/day)(1/cell)
c	2.4	1/day
s_T	$10\times^4$	cells/day
r	0.251	1/day
k_T	3.16×10^4	log10 copies/mL
δ_T	0.1	1/day

On the other hand, for immune response the initial values of the EKF are set as follows: $P_{1,0} = 1 \times 10^6$, $P_{2,0} = 1 \times 10^3$, $Q_1 = Q_2 = 10000$, $R_1 = 100$, $R_2 = 480$, $\eta_1 = 0.91$ and $\eta_2 = 0.5$.

Table 1 presents the parameters taken from patient D presented in [6] with $n = 2$. The initial values of the dynamic system (27)-(28) are $V_0 = 0.31$ copies/mL and $T_0 = 10^6$ cells are set as suggested in [5].

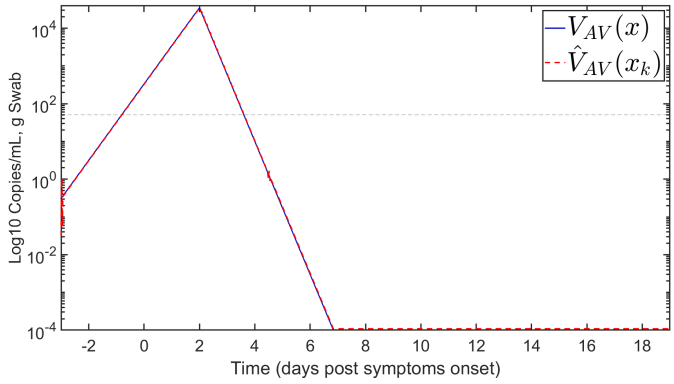

(a) Viral load

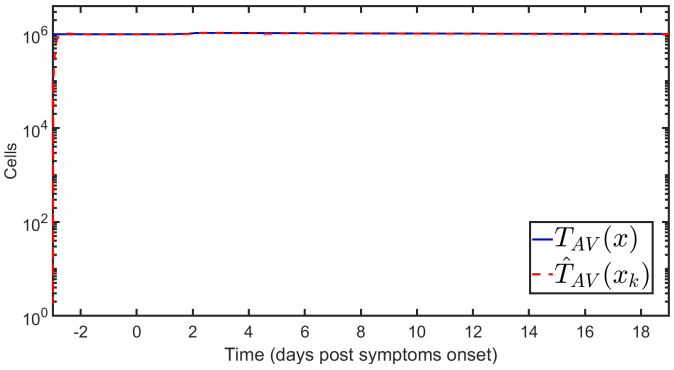

(b) T-cell response

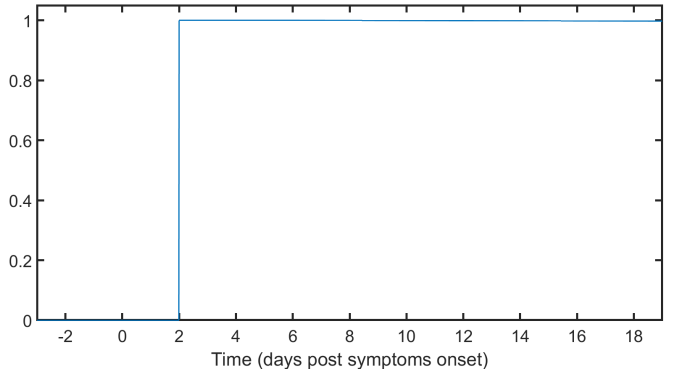

(c) Control law

Fig. 2. **Viral dynamics, T-cell response and control law for antivirals effects**. In figure 2a the blue line represent the continuous system, red dashed line display the neural identifier and black dashed line represent the detectable levels. On the other hand in figure 2b the blue line represent the T-cell response of continuous system and the red dashed line is the neural identifier. Finally in figure 2c the blue line is the neural inverse optimal control law.

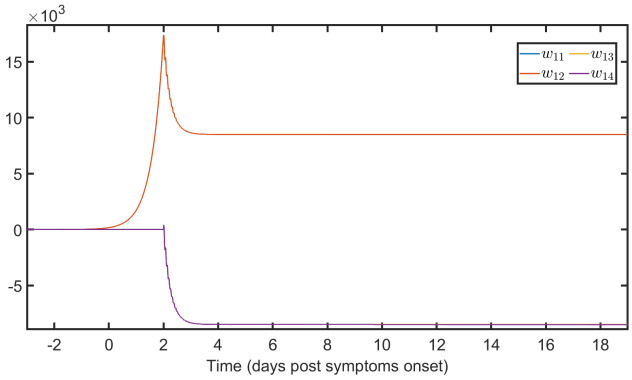

(a) Viral load

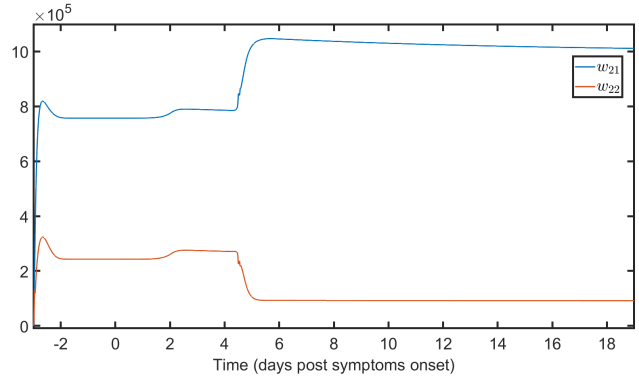

(b) T-cell response

Fig. 3. **RHONN weights of antivirals.** w_{11}, w_{12}, w_{13} and w_{14} are the weights of viral load dynamics, w_{21} and w_{22} are the weights that corresponds to T cell proliferation dynamics.

For simulations the sampling time is established as $T_s = 0.01$. From [5] infection time is assumed at -3 days post symptoms onset, for this reason initial simulation time is setting as $t_0 = -3$.

In antiviral and immune response the control input begins at day 2 post-symptoms onset, as suggested in other viral treatments as in [9]. It should be noted that viral load cannot be measured below detectable levels about 100 copies/mL; in [28] suggests using half of the detection levels about 50 copies/mL.

A. Antivirals Effects

Fig. 2a and 2b present the viral load and T-cell response obtained by antiviral effects, represented in the continuous system as in (27)-(28) with $u_m = 1$ and the neural model presented in (35)-(36); previous systems are using u_r synthesized by the neural inverse optimal control law displayed in Fig. 2c. It can be seen in fig. 2a that the viral load is no longer detectable at day 3.6 post symptoms onset. Fig. 2b displays T cell maximum peak is achieved on day 2.3 post-symptoms onset.

For this controller it was suggested in [29] that it should maintain an effectiveness above 80% to reduce the peak viral load if treatment is applied after symptoms onset. Fig. 2c illustrates that the proposed controller maintains an effectiveness

of approximately 100% until day 19 post symptoms onset. Fig. 3a - 3b presents RHONN weights for model presented in (35)-(36).

B. Immune response effects

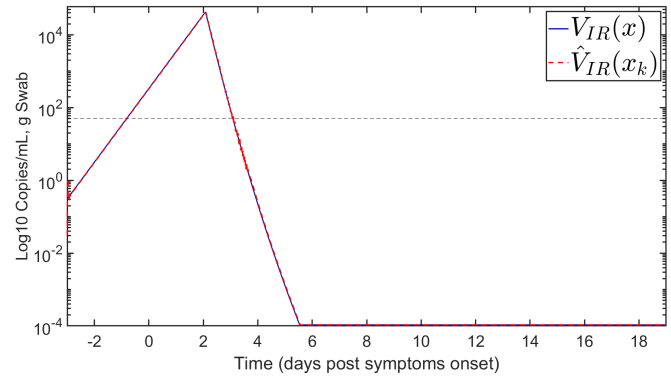

(a) Viral load

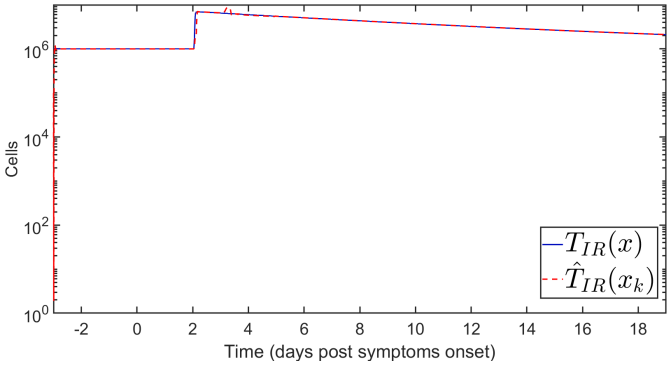

(b) T-cell response

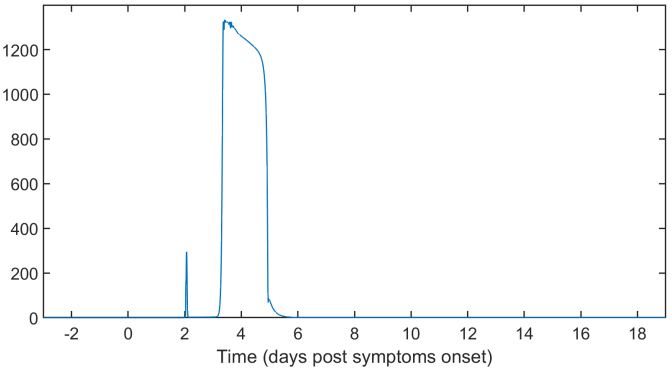

(c) Control law

Fig. 4. **Viral dynamics, T-cell response and control law for immune response effects**. In figure 4a the blue line represent the continuous system, red dashed line display the neural identifier and black dashed line represent the detectable levels . On the other hand in figure 4b the blue line represent the T-cell response of continuous system and the red dashed line is the neural identifier. Finally in figure 4c the blue line is therapy provided by the neural inverse optimal control law.

Viral load and T-cell responses obtained by immune response are presented in Fig. 4a and 4b. Dynamics are represented by continuous system as in (27)-(28) with $u_r = 0$ and the neural model presented in (39)-(40). u_m is synthesized by the neural inverse optimal control law displayed in Fig. 4c. The RHONN weights of (39)-(40) are displayed in Fig. 5.

On day 3.1 post symptoms onset the viral load is no longer detected as shown in fig. 4a. Fig. 4b displays T cell maximum peak is achieved on day 2.1 post-symptoms onset.

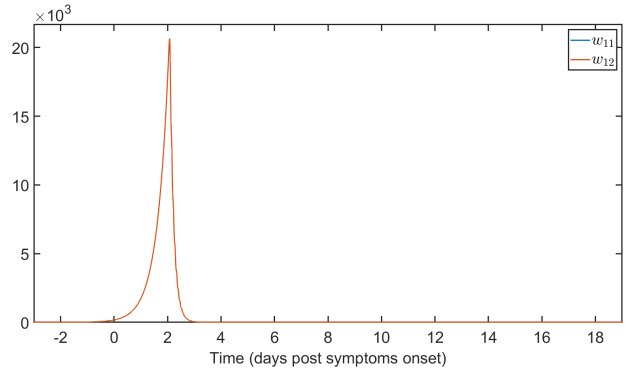

(a) Viral load

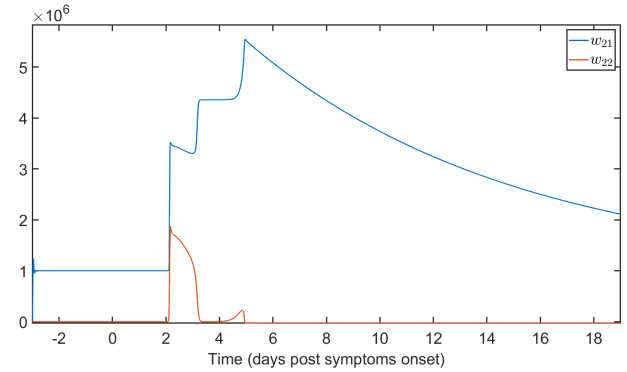

(b) T-cell response

Fig. 5. **RHONN weights of immune response.** w_{11} and w_{12} are the weights of viral load dynamics, w_{21} and w_{22} are the weights that corresponds to T cell proliferation dynamics.

In both cases, a better response time can be observed by decreasing the viral load in a shorter time compared to not having any of these therapies; without these therapies the viral load was no longer detectable until day 12. On the other hand it can also be determined from the results obtained above, that there is a greater number of T cells with the immune response compared to the antiviral effects.

In Fig. 6 it can be observed that there is a difference of approximately half a day in which the viral load is no longer detectable; for that reason the immune response $u_{m,k}$ obtains a better effectiveness compared to the antivirals $u_{r,k}$. Thus, even if there is a 100% effective drug against COVID-19, the results obtained show that a better medical therapy would be to stimulate the immune response.

VI. Conclusions

In this paper a discrete time neural inverse optimal controller is applied for the treatment of patients with COVID-19. For system identification a RHONN is proposed, which is online

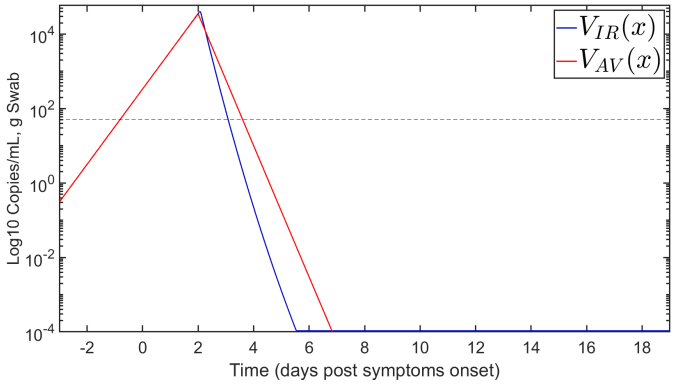

Fig. 6. **Viral load comparison.** Red line displays viral load obtained with only antiviral effects and blue line display the viral load by boosting the immune response effect.

trained with an EKF algorithm. The optimal controller is implemented with antiviral and immune responses. Simulations present the performance of each one control inputs. The immune response effects displays a better performance compared with the one using antivirals. Real-time implementation of these therapies is difficult, as some details such as sampling, measurements and of course the candidate drug that is available for the treatment of this disease have to be solved. Future work will analyze both control inputs in the same system, as well as test other control techniques for this system.

REFERENCES

[1] World Health Organization. WHO Coronavirus Disease (COVID-19) Dashboard. WHO Coronavirus Disease (COVID-19) Dashboard. Retrieved February 1, 2021, from https://covid19.who.int/

[2] Liu, Z., Magal, P., Seydi, O. and Webb., G. "Predicting the cumulative number of cases for the COVID-19 epidemic in China from early data." Mathematical Biosciences and Engineering, 2020, 17(4): 3040-3051. doi: 10.3934/mbe.2020172

[3] Yang, C. and Wang, J "Modeling the transmission of COVID-19 in the US – A case study", Infectious Disease Modelling, Volume 6, 2021, Pages 195-211, https://doi.org/10.1016/j.idm.2020.12.006.

[4] Veera Krishna, M. "Mathematical modelling on diffusion and control of COVID–19", Infectious Disease Modelling, Volume 5, 2020, Pages 588-597, https://doi.org/10.1016/j.idm.2020.08.009.

[5] Hernandez-Vargas, E. A. and Velasco-Hernandez, J. X. "In-host mathematical model of COVID-19 in Humans" Annual Reviews in Control, vol. 50, pp 448-456, 2020. doi:10.1016/j.arcontrol.2020.09.006.

[6] Wölfel, R. and Corman, V.M. and Guggemos, W. et al. "Virological assessment of hospitalized patients with COVID-2019" Nature 581, pp 465–469, 2020

[7] İğret Araz, S. "Analysis of a Covid-19 model: Optimal control, stability and simulations", Alexandria Engineering Journal, Volume 60, Issue 1, 2021, Pages 647-658, https://doi.org/10.1016/j.aej.2020.09.058.

[8] Cao, B. and Kang, T. "Nonlinear adaptive control of COVID-19 with media campaigns and treatment" Biochemical and Biophysical Research Communications, 2021, https://doi.org/10.1016/j.bbrc.2020.12.105.

[9] Hernandez-Mejía, G. and Alanis, A. Y. and Hernandez-Vargas, E. A. "Neural inverse optimal control for discrete-time impulsive systems", Neurocomputing, vol. 314, pp 101-108, 2018.

[10] Hernandez-Vargas, E. A., Middleton, R. H. and Colaneri, P. "Optimal and MPC Switching Strategies for Mitigating Viral Mutation and Escape", IFAC Proceedings Volumes, Volume 44, Issue 1, 2011, Pages 14857-14862, https://doi.org/10.3182/20110828-6-IT-1002.01137.

[11] R. A. Freeman and P. V. Kokotovi, "Robust Nonlinear Control Design: State-Space and Lyapunov Techniques.", Cambridge, MA, USA: Birkhauser Boston Inc., 1996

[12] E. N. Sanchez and F. Ornelas-Tellez, "Discrete-time inverse optimal control for nonlinear systems". Boca Raton, Florida, U.S.: CRC Press, 2013

[13] Rovithakis, G. A. and Chistodoulou, M. A. "Adaptive Control with Recurrent High-Order Neural Networks", Springer, 2000.

[14] E. N. Sanchez, A. Y. Alanis, and A. G. Loukianov, "Discrete-time High Order Neural Control". Berlin, Germany: Springer-Verlag, 2008.

[15] G. Aquino et al., "Novel Nonlinear Hypothesis for the Delta Parallel Robot Modeling," in IEEE Access, vol. 8, pp. 46324-46334, 2020, doi: 10.1109/ACCESS.2020.2979141.

[16] J. de Jesus Rubio, "SOFMLS: Online Self-Organizing Fuzzy Modified Least-Squares Network," in IEEE Transactions on Fuzzy Systems, vol. 17, no. 6, pp. 1296-1309, Dec. 2009, doi: 10.1109/TFUZZ.2009.2029569.

[17] H. -S. Chiang, M. -Y. Chen and Y. -J. Huang, "Wavelet-Based EEG Processing for Epilepsy Detection Using Fuzzy Entropy and Associative Petri Net," in IEEE Access, vol. 7, pp. 103255-103262, 2019, doi: 10.1109/ACCESS.2019.2929266.

[18] J. J. de Rubio, "Stability Analysis of the Modified Levenberg-Marquardt Algorithm for the Artificial Neural Network Training," in IEEE Transactions on Neural Networks and Learning Systems, doi: 10.1109/TNNLS.2020.3015200.

[19] J. A. Meda-Campaña, "On the Estimation and Control of Nonlinear Systems With Parametric Uncertainties and Noisy Outputs," in IEEE Access, vol. 6, pp. 31968-31973, 2018, doi: 10.1109/ACCESS.2018.2846483.

[20] Gerardo Hernández, Erik Zamora, Humberto Sossa, Germán Téllez, Federico Furlán, "Hybrid neural networks for big data classification, " Neurocomputing, Volume 390, 2020, pp. 327-340, ISSN 0925-2312, https://doi.org/10.1016/j.neucom.2019.08.095.

[21] Y. Y. Rios et al., "Inverse Optimal Control Using A Neural Multi-Step Predictor For T1DM Treatment," 2018 International Joint Conference on Neural Networks (IJCNN), Rio de Janeiro, 2018, pp. 1-8, doi: 10.1109/IJCNN.2018.8489197

[22] Alanis, A. Y. and Sánchez, E. N. and Loukianov, A. G. "Discrete-Time Adaptive Backstepping Nonlinear Control via High-Order Neural Networks", in *IEEE Transactions on Neural Networks*, vol. 18, no. 4, pp. 1185-1195, July 2007. doi: 10.1109/TNN.2007.899170

[23] D. E. Kirk, *Optimal Control Theory: An Introduction* Dover Publications Inc., NJ, USA: Prentice-Hall,1970

[24] F. L. Lewis and V.L. Syrmos, *Optimal Control*. New York, NY, USA: John Wiley & Sons, 1995

[25] T. Basar and G.J. Olsder, *Dynamic Noncooperative Game Theory* 2nd ed. New York, NY, USA: Academic Press, 1995

[26] T Ohsawa, A. M. Bloch, and M. Leok, "Discrete Hamilton-Jacobi theory and discrete optimal control" *Proceedings of the 49th IEEE Conference on Decision and Control* (CDC), Atlanta, Ga, USA, Dec. 2010, pp 5438-5443.

[27] A. Al-Tamimi and F. L. Lewis, "Discrete-time nonlinear HJB solution using approximate dynamic programming: Convergence proof", *IEEE Transactions on Systems, Man, Cybernetics-Part B*, vol. 38, no. 4, pp. 943-949, 2008.

[28] Hernandez-Vargas, E. A., Wilk, E., Canini, L., Toapanta, F. R., Binder, S. C., Uvarovskii, A., … Meyer-Hermann, M. (2014b). "Effects of aging on influenza virus infection dynamics." Journal of Virology, 88(8), 4123–4131

[29] Gonçalves, A., Bertrand, J., Ke, R., Comets, E., de Lamballerie, X., Malvy, D., … Guedj, J. (2020). "Timing of antiviral treatment initiation is critical to reduce SARS-Cov-2 viral load". medRxiv. https://doi.org/10.1101/2020.04.04.20047886